1

Context

1.1 Million Suns

The story of Gamma Ray Bursts is one of the most fascinating in the history of astrophysics. They were discovered serendipitously by military satellites. Remaining an enigma for nearly two decades from then on, they allowed large number of theories to float. The source manifests at all wavebands, yet, there are open problems. No other phenomenon can claim such a glamourous biography.

Gamma Ray Bursts (GRBs) are brilliant flashes of radiation, appearing in soft γ-ray band* and lasting for milli seconds to a few hundred seconds. The energy contained in one such flash could amount up to 10^{50} – 10^{51} ergs, which equals the brightness of several million sun like stars. They mark stellar death, or has to do with objects associated with stellar death.

The event, in most† of the cases, appears in two phases: The Burst and the Afterglow. While the burst lasts only for a few seconds and appears only in the γ-ray band, the afterglow (AG) appears in all bands of the electromagnetic spectrum and lasts for months to years (depending on the band).

*100 keV to 1 MeV, in this context

†For some GRBs, afterglow is not detected, which may be due to the intrinsic faintness of the AG or due to the poor information on the burst location which makes follow up activities difficult.

As a preamble to this thesis, a brief sketch of the development and the current status of the field is presented here.

1.1.1 Discovery

Already a much told episode; the discovery of Gamma Ray Bursts (GRBs) is credited to the Vela military satellites, launched by the United States to monitor violation of Nuclear Test Ban Treaty. Kept as a defence secret, the discovery was finally announced in 1973 [78]. Signal from the first GRB detected, GRB640702*, is shown in fig 1.1.

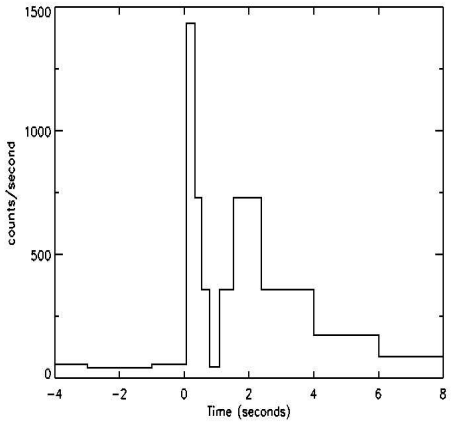

Figure 1.1. The first GRB. The flash appears suddenly and lasts for less than 10 seconds. Reference : [78]

1.1.2 Long & Short

There are two types of bursts. The long ones (l-GRBs) last for more than 2 sec, while the short ones (s-GRBs) fade away within less than a second. Apart from the duration, they also differ in their hardness ratio†. In figure 1.2, the plot of

*The convention is GRByymmdd. *ie.*,this one is detected on 2nd July 1964.

†Ratio of photos observed in one channel (high energetic) to a second one (low energetic).

number vs. duration is presented, clearly depicting the bimodal distribution of the bursts.

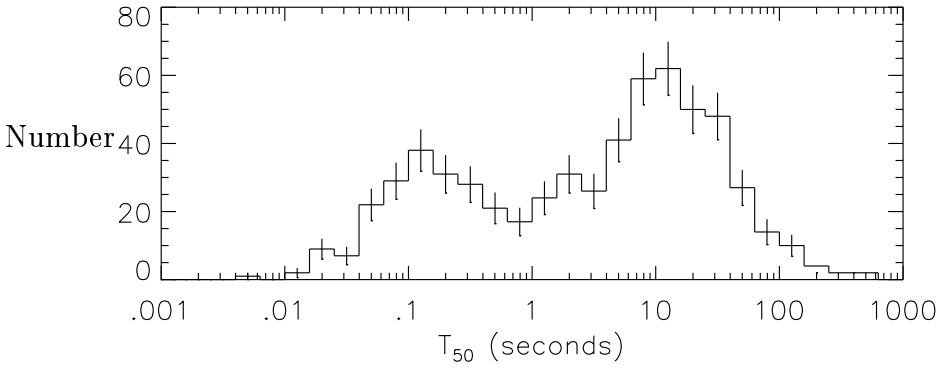

Figure 1.2. Number of bursts, vs. their duration (T_{50} is the time required for the flux to decay to half of the peak value). The distribution is bimodal, with l-GRBs of 10 s to 100 s seconds of duration against s-GRBs with duration less than a second. From [95]

1.1.3 Burst Profile

The temporal profiles vary from burst to burst. In figure 1.3, lightcurves of some of the l-GRBs are shown, the diversity among them is obvious. A typical GRB lightcurve has a Fast-Rise-and-Exponential-Decay (FRED) profile and may contain multiple such components, variabilities in time scales of milliseconds are often observed.

The spectra (fig 1.4) are non-thermal, extending typically from ~ 100 KeV to ~ 1 MeV. The shape can be well explained by the Band function [5], which is a two component power-law joined smoothly at the break.

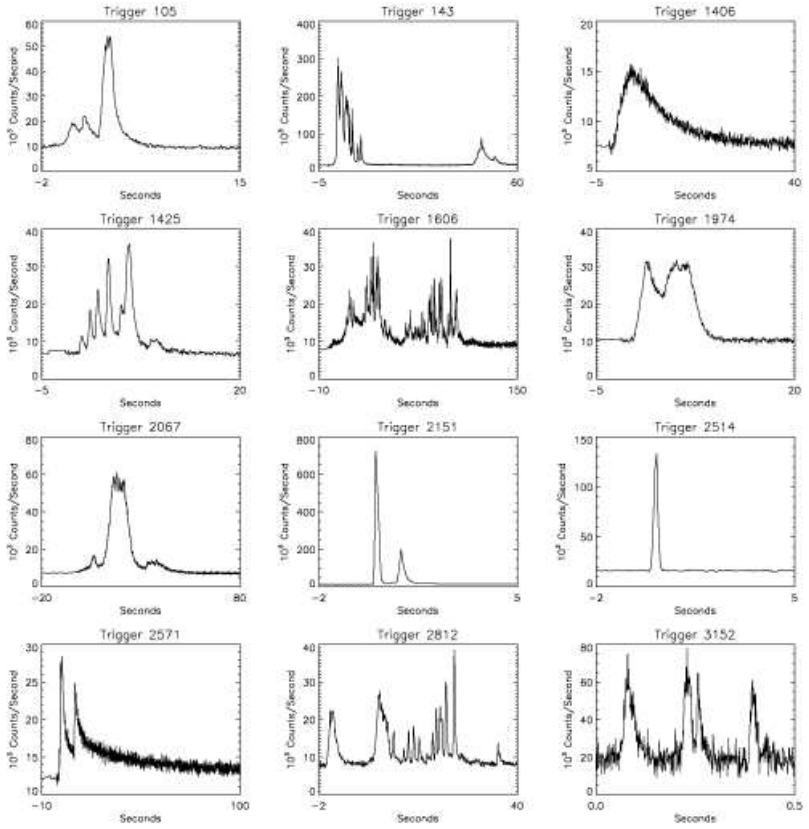

Figure 1.3. Lightcurves of some of the bursts, to display their apparent diversity. While some are single-spiked some display multiple spikes. Some lightcurves are smooth, but some of them are accompanied by subspikes. The presence of multiple spikes was one underlying reason for the 'internal shock' model.

1.1.4 The *Compactness* Problem and Γ_{sh}

The size estimated* using the millisecond variabilities seen in the lightcurves, led to emitting volumes so small, and radiation energy density so large, that the emergence of high energy photons would have been strongly suppressed due to pair production. However, that does not happen and one does observe the γ-ray photons above the threshold of pair production (> 0.5 GeV) from a GRB. The solution to this puzzle came in the form of relativistic bulk motion of the emitting

*using the causality argument : $R = c\Delta t$, where c is the velocity of light and Δt is the variability timescale

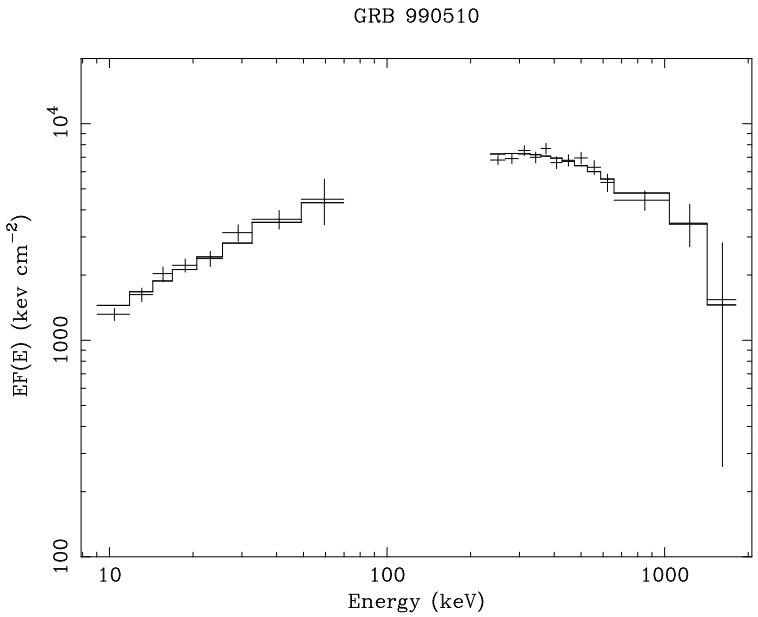

Figure 1.4. A typical burst spectrum. Reference: [3]

plasma [40, 143]. The pair production optical depth τ,

$$\begin{aligned} \tau &= f_p \frac{\sigma_T F d_L^2}{R^2 m_e c^2} \\ &= 4.35 \times 10^{15} f_p \frac{F}{10^{-6}\mathrm{erg/cm^2/sec}} \left[\frac{d_L}{7.12\mathrm{Gpc}}\right]^2 \left[\frac{3000\mathrm{km}}{R}\right]^2 \end{aligned} \tag{1.1}$$

where F is the source flux, gets modified by relativistic bulk motion of the source in the following way.

(i) f_p, the fraction of photons capable of pair production comes down due to doppler boosting.

(ii) R, the size of the emitting region increases due to special relativistic effects.

This brings τ down by a factor of Γ^{-6} where Γ is the bulk lorentz factor of the source, which allows one to see the high energy photons.

The same argument had been used in the context of extra-galactic radio sources too, though the value of Γ required in that case was smaller (~ 10) while GRBs needed the second highest relativistic motion ($\Gamma \sim 100 - 1000$) known in

the astrophysical context*. The observational evidence of the relativistic bulk motion came later, through observations of radio afterglows[141].

1.2 Afterglows

The energy of the explosion is more or less equally divided into its two phases, – the burst carries it in radiation while the afterglow reflects the part which goes into kinetic energy of the ejected matter. Paczynski & Rhoads, in 1993, predicted the possibility of afterglows. The prediction was confirmed later, by the discovery of prolonged emission in x-ray/optical and radio bands associated with the GRB of 1997 February 28th [30, 47, 135]. Until afterglows were revealed, nothing conclusive was known about the nature or origin of Gamma Ray Bursts. Their unexpected appearance followed by the quick disappearance, hindered any detailed study. AGs confirmed the hypothesis of cosmological origin, relativistic bulk motion and the presence of collisionless shocks.

Till late 2004, AGs were detected only for l-GRBs, as a result, detailed study was possible only for this class. However, after the launch of the satellite Swift†, the scenario underwent a major change, and several s-GRBs were followed up in x-ray, optical and radio bands [12, 43, 69, 140].

Collimation : The explosion which makes GRBs is not isotropic, instead is collimated in a narrow cone. This picture emerged first as a prediction [112], which was later confirmed by observations of GRB980519 and GRB990510 ([65, 127] respectively).

The evidence of a collimated outflow is an *achromatic break* seen in the AG light curve. From the time (t_j) at which this break happens, the angle of the cone (θ_0) can be inferred. The mean value of θ_0 is $\sim 4\,\mathrm{deg}$ [48]. Collimation plays an important role in the determination of energetics, rate of occurrence and progenitor models for GRBs and will be discussed in forthcoming sections.

*Pulsar winds, for example that from crab, has $\Gamma \sim 10^6$.

†The NASA-ESO dedicated Gamma Ray Burst mission, launched on 20th November 2004, that has already made several important discoveries.

1.3 Location

GRBs are extragalactic* events happening at cosmological distances. The closest detected so far is GRB980425 at a distance of 39 Mpc ($z = 0.0085$)†. And the farthest is GRB050904 at 66 Gpc ($z = 6.29$) ([32, 64]). The distance is inferred from the spectroscopic redshift of the absorption lines seen against the bright optical afterglow. These lines originate in the intervening medium, mainly in the galaxy where the explosion occurred. Often, the host galaxy is detected and its emission lines further confirm the redshift. Another way of estimating the redshift, especially applied to high redshift bursts (for example, the z of GRB050904 is calculated likewise) makes use of the Lyman limit‡ which gets redshifted and appears in the visible range of the AG spectrum.

For most of the well-localized GRBs, host galaxies were detected in optical band. The reported magnitudes of the hosts are $20.4 < R < 30$. A few hosts are seen in millimeter and radio bands as well. They are usually extremely blue with the presence of young stellar population. Most of them are irregular, suggesting the possibility of past merger episodes. There is increasing evidence that the galaxies are of low metallicity ($Z_\odot/10^4$). This suggests, though not conclusively that GRBs happen in regions that are metal poor.

Being bright and far, GRBs can trace star formation and the early history of the universe much better than any other source can do, which makes them precious beacons of early universe. In figure 1.5, the redshift distribution of GRBs observed by SWIFT is shown.

1.4 Energetics

Using the observed fluence§, f_γ, in the γ-ray band, and the redshift(z) of the source, one can calculate the energy budget of the event in radiation, since most

*So far a GRB has not been observed in our Galaxy, the probability of its occurrence is very low.

†For all calculations, we use $H_0 = 65, \Omega_m = 0.3$ and $\Omega_\Lambda = 0.7$

‡The absorption edge of neutral hydrogen atoms, which corresponds to the largest transition possible, from $n = 1 \to \infty$, $h\nu = 13.6$eV. In the rest frame, this appears in the UV band.

§Fluence is the energy received per unit area per unit frequency, has unit of erg/cm^2/Hz.

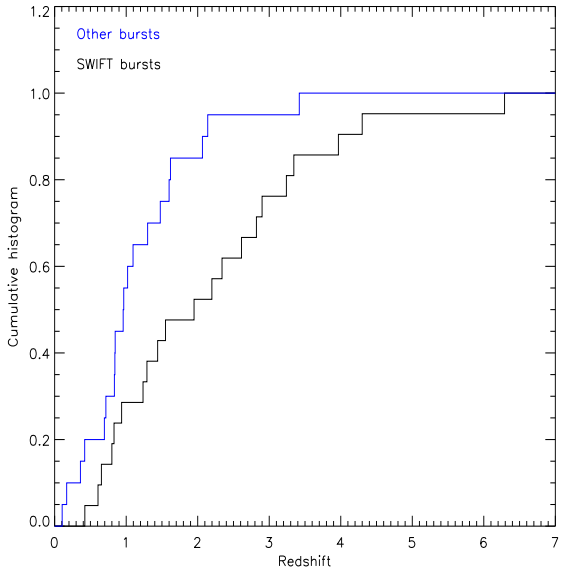

Figure 1.5. The redshift distribution of pre-*Swift*(top) and *Swift* (bottom) bursts [55].

of the energy is emitted in the γ-ray band alone.

$$E_{\rm iso}(\gamma) = 3.0 \times 10^{51}{\rm erg} \left[\frac{2}{1+z}\right] \left[\frac{d_L}{7.12\,{\rm Gpc}}\right]^2 \frac{f_\gamma}{10^{-6}{\rm erg/cm^2/Hz}} \tag{1.2}$$

This is the *isotropic equivalent energy* of the burst, because while making the estimate, the energy is assumed to be distributed isotropically.

Typical bursts have $E_{\rm iso}(\gamma)$ around 10^{53} – 10^{54} ergs. The actual amount of energy involved is less, roughly by a factor of 500 (for typical values of θ_0), if the outflow is collimated.

$$\begin{aligned} E_\gamma &= \frac{\Omega}{4\pi} E_{\rm iso}(\gamma) \\ &= \frac{[1-\cos\theta_0]}{2} E_{\rm iso}(\gamma) \end{aligned} \tag{1.3}$$

where Ω is the solid angle of the outflow.

The energy involved is an order of magnitude higher than the kinetic energy derived for supernova explosions, creating neutron stars. Hence the progenitors were suspected to be black holes or neutron stars.

1.5 Supernova Association

One of the most fascinating aspects of GRBs is their association with another explosion, namely, supernovae. So far the connection is established (as well as expected, theoretically) only between l-GRBs and type Ib/c supernovae. Though not all type Ib/c supernovae are suspected to be associated with GRBs, most or all of the l-GRBs are expected to happen along with supernovae.

The first hint of such an association was given by GRB980425/SN1998bw. The burst was followed by the light of the supernova, in x-ray, optical and in radio bands. No afterglow was seen, hence only a temporal association was conclusive. Later some more AGs showed a *signature* of an underlying supernova ([20, 86]). This *signature* is indicated by a 'reddening' of the afterglow spectrum and a corresponding 'bump' (see figure1.6a) in the lightcurve. The first conclusive evidence came from GRB030329/SN2003dh (see chapter 4 and 5 for a detailed study of this AG) the optical spectrum of which evolved from the featureless continuum of the afterglow to a redder one of the SN, with characteristic emission and absorption lines (see figure1.6b). Recently, GRB060218/SN2006aj showed an evolution similar to GRB030329/SN2003dh (Fatkhullin et al. [39].)

1.6 Progenitors

The progenitors of l-GRBs are believed to be massive stars, which catastrophically die to become blackholes. The association with supernovae emphasises the stellar death theory and the conjecture of the *collapsar* model. The collapsing star produces a blackhole-torus system and the blackhole accretes from the torus and eventually launches a jet. The star should be rotating fast enough to support the formation of torus, by leaving some matter capable of staying outside the event horizon of the blackhole. The jet is launched through the rotation axis of the star.

For an s-GRB, the origin is hypothesised to be the coalescence of two neutron stars in a binary system.

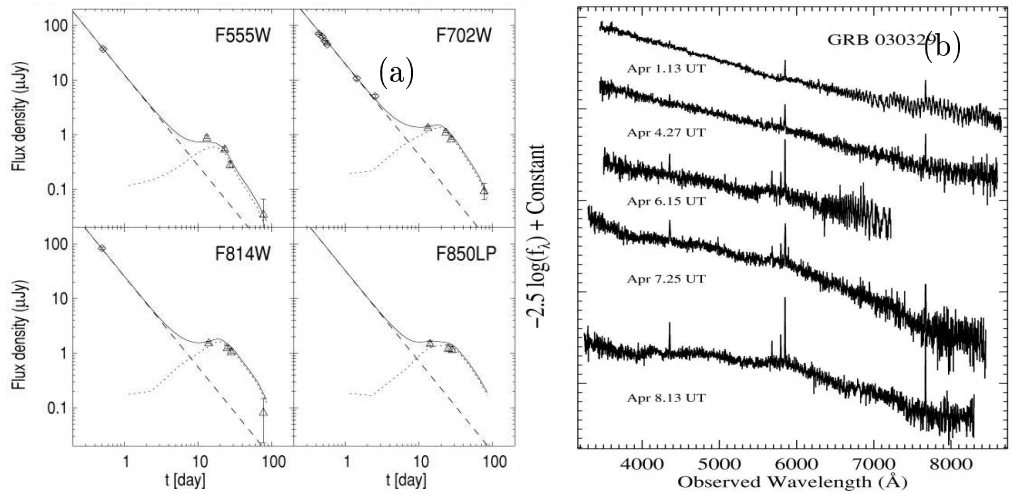

Figure 1.6. Supernova signature: (Left)Indirect evidence: The bump seen in the optical lightcurve, an otherwise monotonous decay of the flux changes to a 'refreshment'. This could occur due to other reasons too, but if this bump is associated with a reddening of the spectrum, a supernova signature is suspected [20]. (Right) Direct evidence : GRB030329, [129], the featureless synchrotron spectrum is taken over by the supernova spectrum.

1.7 Rate

The observed rate of GRBs is $\sim 10^{-7}\mathrm{yr}^{-1}\mathrm{Gal}^{-1}$, from BATSE* observations [146]. However after correcting for collimation, the rate increases by $\frac{4\pi}{\Omega}$ (where Ω is the solid angle within which an observer can see the GRB), which is roughly 500 ([48]) for a typical opening angle. This factor depends on the the assumption of jet profile, since the opening angle is extracted by assuming a geometry of the jet. The rates can also get modified by similar explosions, XRFs†. Hence the possible rate of GRB-XRF events is 10^{-6} – $10^{-7}\mathrm{yr}^{-1}\mathrm{Gal}^{-1}$.

The rate of core-collapse supernovae is $\sim 7 \times 10^{-3}\mathrm{yr}^{-1}\mathrm{Gal}^{-1}$ and that Type Ib/c‡ subclass is roughly 10^{-3} per yr per Galaxy [106]. To compare, the rate

*Burst and Transient Source Experiment, on board Compton Gamma Ray Observatory (1991 – 2000).

†X-Ray Flashes (XRFs) are close allies to GRBs. They have softer spectrum which peaks in the X-ray band.

‡Type Ib/c supernovae are results of single star collapse, like type II. But unlike type II, the compact object formed is conjectured to be a blackhole. The nomenclature comes because of

of massive star formation ($M > 20M_{\odot}$) is in the range of 10^{-4} – 10^{-3} per yr per Galaxy [106]. These values are a few orders of magnitude higher than that of GRB rate, which points out that GRBs are 'special' explosions which require extra conditions than usual core collapse supernovae. This argument has been used in suggesting 'peculiar' progenitor features like presence of binary companion [103] or host environments like low metallicity [144].

The rate of s-GRBs is less certain, due to the lack of proper information about their beaming. Recently more evidence is being gathered, thanks to *Swift* detection of a handful of counterparts, and the rates quoted are $\sim 3 \times 10^{-6}\mathrm{yr}^{-1}$ for the Milky Way [63]. The rate of NS-NS mergers, the supposed progenitors for these class of GRBs, is estimated to be $\sim 10^{-4}\mathrm{yr}^{-1}$ in the Galaxy.

1.8 The Fireball Model

The *standard fireball model*, which involves an 'internal shock' scenario for the bursts and an 'external shock' scenario for the AGs, has been largely successful in explaining the overall behaviour of the burst and the afterglow.

A jet of very little matter and a lot of energy* is launched at speed very close to that of light. The initial lorentz factor could reach upto thousands. The matter in this jet is in the form of shells of varying lorentz factors. Being *cold* (i.e. with negligible internal energy), the energy remains in bulk motion. This energy has to be efficiently converted to kinetic energy of the particles and to radiation. This is achieved through collisionless shocks.

The favourite picture is that the Burst and the *prompt emission*† are due to internal shocks (shocks within the ejected matter) while the afterglow arises from the external shocks (shocks created by the interaction of the ejecta with the surrounding matter).

Internal shocks have been invoked to explain prompt emission, motivated

the absence of hydrogen and helium lines as well as silicon lines. The absence of these elements implies stripping of the outer layers of the exploding star, probably due to severe mass loss.

*In the 'kinetic energy dominated' model. An alternate model exists, in which the jet consists of poynting flux alone.

†Emission in any wavelength simultaneous to the burst.

primarily by complicated lightcurves of GRBs. In the model, the variability of roughly milli-second duration is produced by multiple internal shocks. A picture in which external shocks are invoked for the burst as well as for the AG also exists [36]. In the internal shock model, within the collimated outflow, layers of different lorentz factors catch up with each other and collide, creating multiple shocks. This happens typically 10^{15} – 10^{16} cm away from the exploding star. The internal shocks need not be relativistic, because in the co-moving frame of one layer, the other has only a moderate velocity, even though in the rest frame of the observer both are relativistic. The mechanism for radiation production is the same in both external and internal shocks, but a drawback of the internal shock model is a relatively poor γ-ray production.

The layers after collision, within the shell, form a single entity (details of the mixing of these shells, their energy-mass distribution, etc. are not well studied, but only assumed). This ejecta travels into the ambient medium of the star. As it hits the surrounding medium, a system of *forward and reverse shock* develops. The reverse shock (RS) propagates into the ejecta sweeping up the ejected matter itself. The forward shock (FS) moves into the ambient medium forming a downstream of swept-up ambient matter. The two shocks are separated by a contact discontinuity (CD) (see figure 1.7). The afterglow originates from this system of shocks. Emission from RS is short lived, in those rare cases where it is detected (for example the optical flash of GRB990123 and GRB011211). It quickly falls below the dominating FS emission.

The deceleration radius $r_{\rm dec}$ is defined as the radius at which the inertia of the swept-up mass equals the ejected rest mass $M_{\rm ej}$. If the rest mass of swept up material equals $m(r)$, its inertia will be $\Gamma(r)m(r)$, since the kinetic energy of the relative motion between the unshocked matter and the shock is converted to the internal energy of the matter after being swept up, and contributes to its inertia. As one does not expect considerable reduction of the lorentz factor till $r_{\rm dec}$, $\Gamma(r_{\rm dec})$ essentially equals Γ_0. Equating $\Gamma(r)m(r)$ to $M_{\rm ej}$ (which can be written in terms of the total energy and lorentz factor as $E_{\rm tot}/(\Gamma_0 c^2)$, where Γ_0

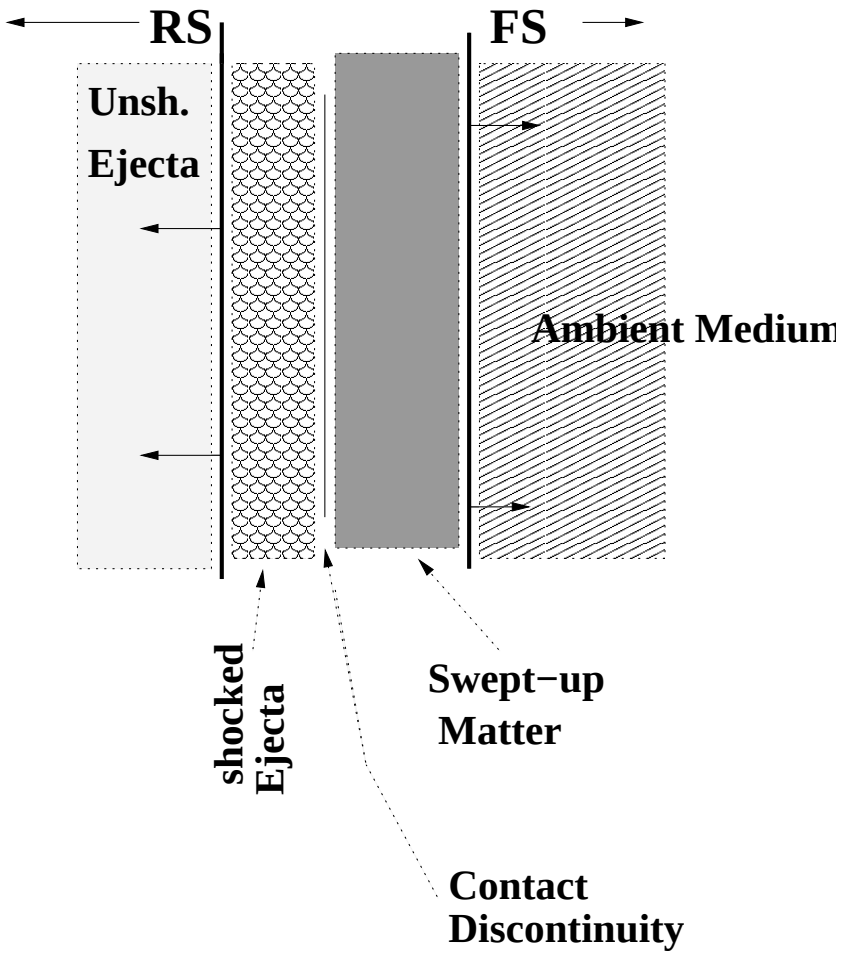

Figure 1.7. A cartoon of the reverse shock forward shock system. The regions are not to scale. For details see section 1.8

is the initial lorentz factor of the ejecta), one obtains

$$r_{\rm dec} = \left[\frac{3}{4\pi c^2 m_p}\right]^{1/3} \left[\frac{\mathcal{E}_{\rm iso}}{n_0 \Gamma_0^2}\right] \tag{1.4}$$

for a constant density ambient medium. The typical $r_{\rm dec}$ is around 10^{17} cm from the onset of the explosion.

1.8.1 External shocks – Shock jump conditions

The shock creates a discontinuity in the thermodynamic variables and the velocity of the medium it propagates through. Behind the front, the shocked matter (downstream) is compressed and heated up. The equations governing the relation between the upstream (undisturbed medium : subscript 1) and downstream (subscript 2) parameters are called *Rankine-Hugoniot* jump conditions.

For a relativistic shock front, which runs into a cold stationary upstream medium, these equations lead to:

$$\begin{aligned} n_2 &\approx 4\Gamma n_1 \\ u_2 &\approx 4\Gamma^2 n_1 m_p c^2 \end{aligned} \tag{1.5}$$

where n is the number density of the medium, u is the energy density of the medium and Γ is the bulk lorentz factor of the shock front. These jump conditions can be used for the FS (with the ambient medium as upstream and swept-up matter as downstream) and for the RS (the unshocked ejecta as the upstream and the shocked ejecta as the downstream)

The assumptions made here are, (i) the plasma is a monoatomic gas, (ii) $\Gamma \gg 1$ and (iii) the downstream matter has the same velocity as the shock front (in reality it will be a little smaller)

1.8.2 External shocks – Timescales

Since there is relative motion involved, special relativistic effects complicate the timescales involved in the problem. There are three timescales of importance, each of them are measured from the time of the explosion.

- $t_\star$ is with respect to the exploding star, and is defined by $dt_\star = dr/c$, where r is the distance from the exploding star.
- $t_{\rm co}$ is the timescale in the frame of the matter moving with the shock (co-moving frame). $dt_{\rm co} = dr/(\Gamma c)$
- $t_{\rm obs}$ or simply t is the earth bound observer's (also the ambient medium's) time.

$$dt_{\rm obs} = dr/(2\Gamma^2 c) \tag{1.6}$$

for $\Gamma \gg 1$ and $\beta \sim 1$

1.8.3 External shocks – dynamics

Blandford & McKee, in 1976, derived the self-similar BM profile for an ultra-relativistic shock decelerating into a medium. The dynamics of the shock is chiefly decided by the density profile of the medium into which it decelerates. It also depends on the radiative losses from the hot downstream plasma.

For afterglow science, one usually considers two types of density profiles. (i) constant density where $\rho(r)$ does not depend on r. This can be identified as the interstellar medium (ISM) or a bubble around the exploding star, created by its own wind. A modification of this profile with small scale density inhomogeneities superimposed is sometimes required to explain variabilities in AG lightcurves ([92]). (ii) $\rho(r) \propto r^{-2}$, which is typical of a stellar wind created density structure. Such a medium is expected around massive stars as they have considerable amount of stellar wind. The density profile can be generalised by introducing a parameter s, as $\rho(r) \propto r^{-s}$. The decay of the lorentz factor with radius of the fireball and the evolution radius with time are dependent on the value of s.

The second factor, the amount of heat escaping from the expanding matter is parametrised as ϵ, defined as the fraction of shock created thermal energy radiated away from the system. The two limiting cases of ϵ are 0 for the *adiabatic evolution* where the radiative losses are negligible and 1 for *radiative evolution* where considerable amount of energy appears in the form of radiation. Afterglows appear to be more commonly seen in the adiabatic phase of evolution. However, it has to be mentioned that ϵ may be a fraction, and it may evolve with time - calculations with such assumptions already exist in literature.

Having parameterised the density profile of the ambient medium and fractional energy release of the shock, one solves the energy-momentum equation (equation 1.1) of the relativistic shock to obtain Γ as function of r.

$$\frac{d\Gamma}{\Gamma^2} - 1 = -\frac{dm}{M} \tag{1.7}$$

where M is the total mass (rest mass + matter equivalent of thermal energy,

since the matter is hot) of the shocked medium in its co-moving frame (which has a lorentz factor Γ w.r.t. the observer's frame) and is given by

$$dM = (1 - \epsilon)dE + dm \tag{1.8}$$

where dE is the incremental thermal energy in the shock down stream ($dE = (\Gamma - 1)dmc^2$) and dm is the incremental swept up mass given by,

$$\frac{dm}{dr} = \Omega(r)r^2 n(r) \tag{1.9}$$

Ω, the solid angle subtended by the ejecta is given as $\Omega = 2\pi(1 - cos(\theta_j))$

The constants of integration will contain the two unknowns, (i) the density of the ambient medium and (ii) the energy content of the explosion.

Jet break and lateral expansion:
The ejected matter is initially collimated in a cone, as mentioned in section 1.2. However, apart from the forward (radial) flow, the matter inside the jet also flows laterally, causing the jet to expand. The jet opening angle gradually grows from the initial value θ_0. In a simplistic approximation, the lateral expansion can be quantified as lateral velocity (which is the speed of sound, c_s in the medium, often equated to c or $c/\sqrt{(3)}$) times the time (t_{co}) elapsed in the rest frame of the jet.

In the co-moving frame, the jet break time $t_{j,co}$ will be that when the lateral expansion starts to dominate the fireball dynamics.

$$c_s t_{j,co} = r_j \theta_0 \tag{1.10}$$

which gives, t_j to be $\propto (\mathcal{E}_{iso}/n)^{1/3}$. This expression is used in deriving θ_0 in terms of $t_j, \mathcal{E}_{iso}$ and n.

Due to the increased working surface of the shock front past jet break, the rate at which matter is encountered by the shock increases and hence the deceleration also increases.

Using the equation of $r(t, \Gamma)$, described in the previous section, Γ is expressed in terms of t. In a constant density medium, an adiabatic blastwave will decelerate according to the scaling law, $\Gamma \propto r^{-3/2}$ before jet break. The radius r will increase as $t^{1/4}$ and hence Γ will be $\propto t^{-3/8}$. After jet break, in approximate solutions,

r remains constant and the density profile will not affect the deceleration. For adiabatic blastwaves, Γ falls as $t^{-1/2}$ past jet break.

A radiative blastwave decelerates as $\Gamma \propto r^{-3}$ and its radius increases as $t^{1/7}$ which results in a $\Gamma \propto t^{-3/7}$ temporal profile. For the wind driven density profiles, $r \propto t^{1/2}$ for $\epsilon = 0$ and $r \propto t^{1/3}$ for $\epsilon = 1$, which results in $\Gamma \propto t^{-1/4}$ and $t^{-1/3}$ respectively.

For a detailed treatment of the (adiabatic) dynamics see chapter 2 of the thesis.

Non-relativistic transition :
The fireball decelerates, and eventually enters the newtonian regime. Here the Blandford-McKee solution gives way to the Sedov-Taylor solution, which is the well known profile seen in supernova remnants. The non-relativistic transition happens when the rest energy of the swept up matter equals the total kinetic energy of the ejected mass. The transition takes place in time scale of months.

The signature of newtonian transition is usually seen in radio afterglow observations [50, 111], since only in radio band the afterglow remains visible sufficiently long.

1.8.4 Particle Acceleration in collisionless shocks

Shocks are ubiquitous in astrophysical systems – they extend from the inter planetary medium to clusters of galaxies. So are the relativistic electrons accelerated by these shocks. Diffusive Shock Acceleration (DSA), a variant of the first order Fermi process for accelerating particles in collisionless shocks ([41]), seems to be a successful candidate in explaining the non-thermal distribution of relativistic electrons encountered in astrophysical sources [9, 19].

The process assumes that the scattering mean free path of the particles are larger than the shock thickness, hence they will be able to criss-cross the shock front repeatedly. In each crossing the particle gains momentum. After each crossing cycle, there is an escape probability ($\mathcal{P}_{\rm esc}$) of the particle being convected away downstream. The momentum gain and the escape probability compete to yield a steady state distribution, which is a power-law in energy, characterised by

an index p.

The power-law distribution can be expressed as,

$$N(E)dE \propto E^{-p}dE \tag{1.11}$$

where

$$p = 1 + \frac{\ln 1/\mathcal{P}_{\rm ret}}{\ln E_f/E_i} \tag{1.12}$$

where $\mathcal{P}_{\rm ret} = 1 - \mathcal{P}_{\rm esc}$ and E_f/E_i is the factor by which the particle gains energy in each cycle.

1.8.5 Synchrotron Radiation and Afterglow Spectra

It is understood that most of the afterglow radiation received in all bands arise from the synchrotron process. The electrons which are accelerated to high energies by DSA will gyrate around the shock-amplified magnetic field and produce synchrotron emission. Compton emission due to the upscattering of these synchrotron photons by the same electrons (Synchrotron Self Compton or SSA) could also play a role, but only at high frequencies.

The frequency integrated power emitted by a single electron due to synchrotron radiation is given by

$$P(\gamma) = \frac{\sigma_T c}{6\pi} B^2\gamma^2 \tag{1.13}$$

where γ is the lorentz factor of the electron (different from Γ, the bulk lorentz factor of the moving plasma) and B is the magnetic field.

It has to be noted that the power emitted is proportional to the square of the electron lorentz factor, which implies that the higher the energy, the greater is the synchrotron loss.

The expression for the characteristic synchrotron frequency $\nu_{\rm ch}$ of an electron of lorentz factor γ is given as,

$$\nu_{\rm ch}(\gamma) = \frac{3e}{4\pi m_e c}\gamma^2 B \tag{1.14}$$

The spectrum, $P(\nu,\gamma)$ initially rises, as a powerlaw proportional to $\nu^{1/3}$, peaks at a frequency which is 0.29 times $\nu_{\rm ch}$, then falls of exponentially.

$$P(\nu,\gamma) = \sqrt{3}\frac{e^3 B}{m_e c^2} F(x) \tag{1.15}$$

where $F(x)$, the dimensionless function of $x = \frac{\nu}{\nu_{\rm ch}}$ carries the frequency dependence of the power.

In the asymptotic limits, it can be represented as

$$F(x) \sim \begin{cases} \frac{4\pi}{\sqrt{3}\Gamma\left(\frac{1}{3}\right)} \left(\frac{x}{2}\right)^{1/3} & x << 1 \\ \left(\frac{\pi}{2}\right)^{1/2} \exp -x\, x^{1/2} & x >> 1 \end{cases} \tag{1.16}$$

However, the plasma contains electrons of not just a single energy, but a distribution of energies, as introduced in equation 1.11. The total energy in this distribution of relativistic electrons comes at the expense of a fraction ϵ_e of the downstream thermal energy u (see equation 1.5). Another fraction ϵ_B of the thermal energy goes into the enhanced downstream magnetic field. The values of ϵ_e and ϵ_B cannot, at present, be be predicted from a basic theory, but both of course would have an upper bound of unity.

$$\begin{aligned} u_e &= \epsilon_e 4\Gamma^2 n m_p c^2 \\ u_B &= \epsilon_B 4\Gamma^2 n m_p c^2 \end{aligned} \tag{1.17}$$

1.8.6 Electron energy distribution function

The energy distribution introduced in equation 1.11 is characterised by at least three parameters : the power-law index (p) and a minimum value of energy $\gamma_m m_e c^2$ and an upper cutoff energy $\gamma_u m_e c^2$.

$$N(\gamma)d\gamma = K_e \gamma^{-p} d\gamma \qquad \text{where, } \gamma_m \le \gamma \le \gamma_u \tag{1.18}$$

where we have used lorentz factor to represent energy ($E = \gamma m_e c^2$)

The energy contained in this distribution is,

$$u = K_e m_e c^2 \frac{\gamma_m^{-(p-2)} - \gamma_u^{-(p-2)}}{p-2} \tag{1.19}$$

As the standard model assumes that $p > 2$, the term containing γ_u in equation 1.19 can be neglected when $\gamma_u \gg \gamma_m$, simplifying the algebra to a large extent and reducing the number of unknown parameters by two. In this approximation, γ_m will be,

$$\gamma_m = \frac{p-2}{p-1}\frac{m_p}{m_e}\epsilon_e\Gamma \tag{1.20}$$

It should be mentioned that numerical simulations of DSA process tend to predict an universal value of p that is larger than 2.0. Besides, well studied Galactic supernova remnants, where non-relativistic shocks come into play, often exhibit $p \sim 2.2 - 2.5$. However this need not always be true, we deal with this issue in detail in chapter 4 & 3

The integrated emission from such a distribution can be approximated as segmented powerlaws joined at breaks.

1.8.7 Spectral Breaks

The synchrotron spectrum from a population of particles, distributed in a power-law described in eqn. (1.7) rises with frequency and peaks at the characteristic frequency, $\nu_{\rm ch}(\gamma_m)$ corresponding to the minimum lorentz factor of the distribution γ_m, and falls off at higher frequencies as a power law of slope $-(p-1)/2$. In the observer's frame, the expression for ν_m is given by

$$\nu_m = \frac{x_p}{2\pi m_e c} B\gamma_m^2\Gamma \tag{1.21}$$

which includes the doppler boost and x_p, which is a p dependent factor [142].

The injected electron spectrum, which is given by equation (1.7), evolves due to the energy being radiated away by the synchrotron process. As mentioned earlier, the electrons which are more energetic lose more energy to synchrotron radiation. Energy distribution of electrons for which synchrotron loss dominates, is a powerlaw steeper by an index 1 with respect to the injected energy spectrum, yielding a $\gamma^{-(p+1)}$ distribution.

The loss becomes considerable only for those electrons with radiative timescale ($t_{\rm rad}$: which is a function of energy) below the age ($t_{\rm co}$) of the system. The energy at which this happens can be calculated in the following way : $t_{\rm rad} \equiv \frac{E}{dE/dt} \leq t_{\rm co}$

Hence, γ_c can be derived as $\frac{6\pi m_e c}{\sigma_T}\frac{1}{B^2 t_{\rm co}}$ in the co-moving frame. Written in terms of the observer's time t, this is,

$$\gamma_c = \frac{6\pi m_e c}{\sigma_T}\frac{1}{B^2\Gamma t} \tag{1.22}$$

This steepening in the *accumulated* electron spectrum will be reflected in the radiation spectrum as well. The corresponding "cooling break" in the observed radiation spectrum, is located at the frequency,

$$\nu_c = \frac{0.286}{2\pi m_e c} B\gamma_c^2\Gamma \tag{1.23}$$

Most often, the cooling break appears, in the high frequency bands, such as x-rays or ultra-violet.

The situation discussed above is called *slow cooling*. However, if all the electrons in the distribution are cooling dominated (*ie.*,$\gamma_c < \gamma_m$), the corresponding "fast cooling" electron energy spectrum would have a slope of $-(p+1)$ above γ_m, but in the range $\gamma_c \leq \gamma \leq \gamma_m$, the slope will be -2.

Another break the synchrotron spectrum exhibits, which appears mainly at the low frequency end, arises due to the *self absorption* process. The absorption coefficient $\alpha'_{\nu'}$ for the synchrotron process can be written as,

$$\alpha'_{\nu'} = \frac{(p+2)}{8\pi m_e \nu'^2}\int d\gamma P(\nu',\gamma)\frac{N(\gamma)}{\gamma} \tag{1.24}$$

([114] eqn. (6.52)).

Below the peak frequency ν'_m, where the spectrum follows a 1/3 powerlaw,

$$\begin{aligned} \alpha'_{\nu'} &= \tfrac{p+2}{p+2/3}\tfrac{1}{2\,\Gamma\left(\frac{1}{3}\right)}\tfrac{2\pi e^8}{3(m_e c)^5} K_e \gamma_m^{-(p+2/3)} B^{2/3}\,\nu'^{-5/3} \\ &= C_1 K_e B^{2/3}\gamma_m^{-(p+2/3)}\,\nu'^{-5/3} \end{aligned} \tag{1.25}$$

If $\nu' > \nu_m{}'$,

$$\begin{aligned} \alpha'_{\nu'} &= \tfrac{\sqrt{3}e^3c^2}{8\pi\,(m_e c^2)^{2p}} K_e \left[\tfrac{3e}{2\pi m_e c}\right]^{p/2} \Gamma\left(\tfrac{3p_1+2}{12}\right)\,\Gamma\left(\tfrac{3p_1+22}{12}\right) B^{(p+2)/2}\nu'^{-(p+4)/2} \\ &= C_2 K_e B^{(p+2)/2}\,\nu'^{-(p+4)/2} \end{aligned} \tag{1.26}$$

C_1 and C_2 above are coefficients involving fundamental and numerical constants. Equation (1.25) is equivalent to the result of Rybicki & Lightman, eqn. (6.53)

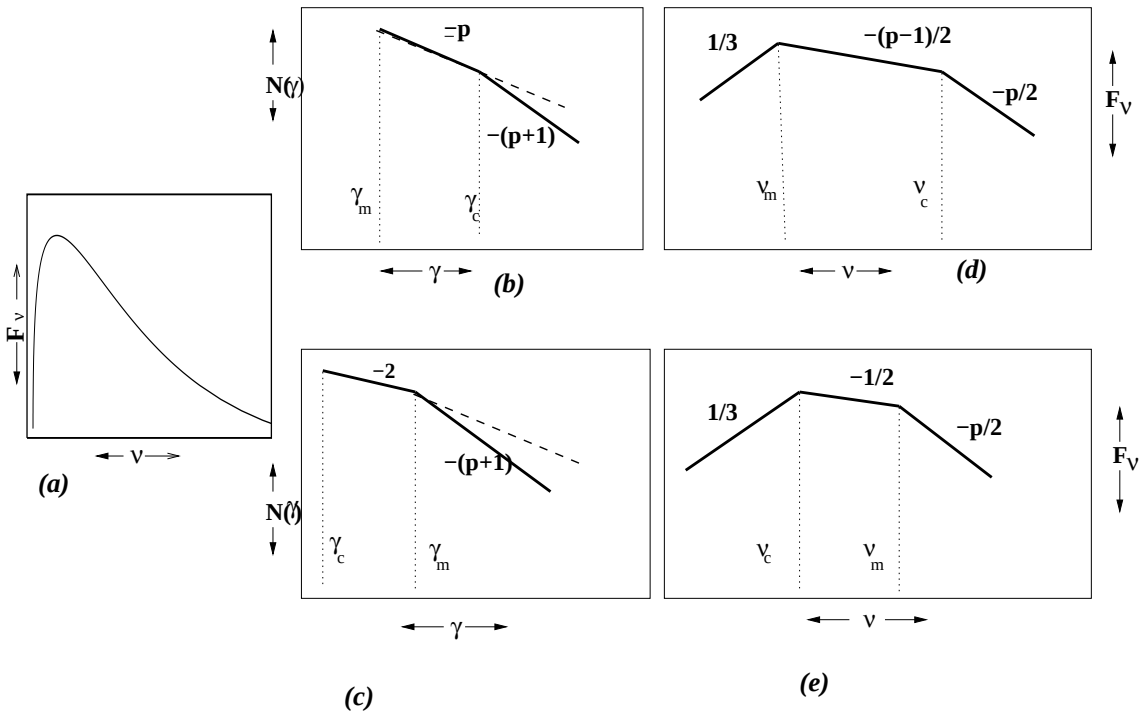

Figure 1.8. Schematic description of synchrotron spectrum in context of section 1.8.7. Panel (a) is the synchrotron spectrum of a mono-energetic electron, which in presence of electron energy distributions displayed in panels (b) and (c), produces radiation spectra shown in panels (d) and (e) respectively. Panels (b) and (d) correspond to slow cooling and panels (c) and (e) to the fast cooling regime. The 'accumulated' energy spectra are shown as solid lines, while 'injected' energy spectra are shown as dashed lines.

In both cases, α_ν decreases with increasing ν, hence the emitting plasma will be optically thick to the low energy photons (self absorption) until the optical depth $\tau'_{\nu'} = \alpha'_{\nu'}\,\Delta'$ becomes unity*. A good approximation of Δ' is to equate it to $a\,R/\Gamma$ where $a \sim 10$.

One can now derive the expression for the synchrotron self absorption frequency ν_a, for both $\nu_a < \nu_m$ (using eqn. 1.26) and $\nu_a > \nu_m$ (using eqn. 1.25).

*Δ' is the distance traveled by the photon, in this particular case of GRB fireballs, it will be the thickness of the emitting plasma in the co-moving frame.

$$\nu_a = \begin{cases} \Gamma\,(C_1 a)^{3/5}\,\gamma_m^{-\frac{3p+2}{5}}\,K_e^{3/5}\,B^{2/5}\,\left(\frac{r}{\Gamma}\right)^{3/5} & \text{If } \nu_a < \nu_m \\ \Gamma\,(C_2 a)^{2/(p+4)}\,B^{\frac{p+2}{p+4}}\,K_e^{2/(p+4)}\,\left(\frac{r}{\Gamma}\right)^{2/(p+4)} & \text{If } \nu_a > \nu_m \end{cases} \tag{1.27}$$

It can be seen from the above expressions that, ν_a depends on the size of the emitting region (here, the radius of the fireball) as well as strongly on the density of the region. In GRB afterglows ν_a therefore provides significant information about the ambient medium as well as the dynamics of the fireball, as we shall see in chapter 5.

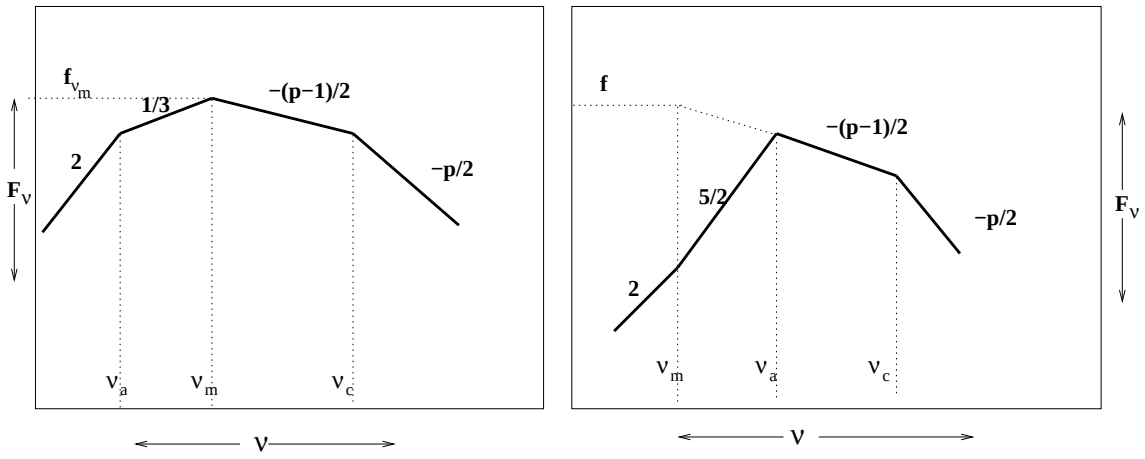

Figure 1.9. Synchrotron self absorption demonstrated for the slow cooling spectrum. In the left panel, the self absorption frequency is below ν_m, and in the right panel $\nu_a > \nu_m$.

The fourth parameter, after ν_m, ν_c and ν_a, in defining the spectrum is f_{ν_m}, the flux at $\nu = \nu_m$. For the afterglow fireball, f_{ν_m} can be written following [142] as,

$$f_{\nu_m} = \frac{N_e \Gamma P_{\nu_m}(1+z)}{\Omega(r) d_L^2} \tag{1.28}$$

where N_e is the total number of electrons in the swept up matter, given by, $\int_0^R \Omega(r) r^2 n(r) dr$, $\Omega(r)$ is the solid angle subtended by the ejecta-cone.

Wijers & Galama (1999), derive P_{ν_m}, power emitted at frequency ν_m to be $\phi_p \frac{\sqrt{3} e^3 B}{m_e c^2}$where ϕ_p is a numerical constant depending on the value of p.

The evolution of an afterglow can be described entirely by these "spectral parameters" (equation 1.21 ,1.23, 1.25, 1.27 and 1.28), in addition to p and the jet break time t_j. These are the observables containing all the information. Four important physical parameters, namely, $\mathcal{E}_{\rm iso}, n(r), \epsilon_e$ and ϵ_B can be derived from the measured values of ν_m, ν_c, ν_a and f_{ν_m}. Using $\mathcal{E}_{\rm iso}$ and t_j, θ_0 and hence $E_{\rm tot}$ are estimated.

The energy distribution index p is obtained from a consistent description of the observed spectral slope in different bands as well as the decay rates of the corresponding lightcurves. This will be explained in the next section.

1.8.8 Importance of multiband observations and modelling

The spectral parameters of an expanding fireball evolves with time, driven by the changing values of Γ, R and B. One can derive these time dependencies for any given dynamical regime of the afterglow. The time evolution of the four spectral parameters for an adiabatic slow cooling fireball is shown below.

Uniform density interstellar medium (ISM)				r^{-2} Wind medium (WIND)			
	$t < t_j$	$t > t_j$			$t < t_j$	$t > t_j$	
ν_m	$t^{-3/2}$	t^{-2}		ν_m	$t^{-3/2}$	t^{-2}	
ν_c	$t^{-1/2}$	t^{0}		ν_c	$t^{+1/2}$	t^{0}	
ν_a	t^{0}	$t^{-1/5}$	(If $\nu_a < \nu_m$)	ν_a	$t^{-3/5}$	$t^{-1/5}$	(If $\nu_a < \nu_m$)
	$t^{-\frac{(3p+2)}{2(p+4)}}$	$t^{-\frac{2(p+1)}{(p+4)}}$	(If $\nu_a > \nu_m$)		$t^{-\frac{3}{2}\frac{(2+p)}{(4+p)}}$	$t^{-\frac{2(p+1)}{(p+4)}}$	(If $\nu_a > \nu_m$)
f_{ν_m}	t^{0}	t^{-1}		f_{ν_m}	$t^{-1/2}$	t^{-1}	

Since the spectrum follows a piecewise powerlaw behaviour in frequency, the

model flux is written in terms of powerlaws appropriate for each spectral regime.

$$f_\nu = \begin{cases} f_{\nu_m} \left(\frac{\nu_a}{\nu_m}\right)^{1/3} \left(\frac{\nu}{\nu_a}\right)^2 & (\nu < \nu_a) \\ f_{\nu_m} \left(\frac{\nu}{\nu_m}\right)^{1/3} & (\nu_a < \nu < \nu_m) \\ f_{\nu_m} \left(\frac{\nu}{\nu_m}\right)^{-(p-1)/2} & (\nu_m < \nu < \nu_c) \\ f_{\nu_m} \left(\frac{\nu_c}{\nu_m}\right)^{-(p-1)/2} \left(\frac{\nu}{\nu_c}\right)^{-p/2} & (\nu_c < \nu) \end{cases} \tag{1.29}$$

Using these temporal dependences of the spectral parameters, one can derive the lightcurve at a given frequency. The expected flux hence can be written as, $f_\nu \propto \nu^\delta t^\alpha$, with δ and α taking on different values in different spectral regimes.

The αs for an adiabatic slow cooling blastwave in various spectral regimes are the following (α_1 is the pre jet break index while α_2 is the post break index)

spectral segment	α_1 (ISM,WIND)	α_2
$\nu_< \nu_a$	1/2, 1	0
$\nu_a < \nu < \nu_m$	1/2, 0	$-1/3$
$\nu_m < \nu < \nu_a$	5/4, 1	1
$\nu_m < \nu < \nu_c$	$-\frac{3(p-1)}{4}$, $-\frac{(3p-1)}{4}$	$-p$
$\nu_c < \nu$	$-\frac{3p-2}{4}$, $-\frac{3p-2}{4}$	$-p$

The value of p appears in the spectral slope as well as in the lightcurve index. Extracting p from optical spectrum is often difficult due to the unknown extinction the afterglow suffers in its host galaxy. The post jet break lightcurve slope equals p, so inference in this way is easier, provided one identifies the jet break. Usually the value is confirmed by looking at the consistency of optical and x-ray spectral indices, and lightcurve slopes.

Due to the time varying spectral parameters, one must monitor the afterglow flux over a long range of time to obtain the full picture. Also, since the spectrum span a wide range of frequencies (from radio to x-ray), monitoring in a large range of frequencies is required. For example, ν_c typically falls in x-rays, or in optical in the early stages of the afterglow, while ν_m is usually found to be located in millimeter or radio bands. The signature of ν_a is found only in radio bands. The full physical picture of the fireball can be retrieved only by multiband modelling of a rich spectral & temporal data set (see chapter 3 & 5 for modelling and physical parameter extraction of well monitored AGs).

1.9 Some Unanswered Questions

Despite a decade of intensive study, many open questions still remain in GRB afterglow evolution. Several observed features remain unexplained, and several physical processes remain poorly understood. We list a few of them, relevant to this thesis.

The afterglow modelling still depends on the simplistic assumptions of fireball model. The 'toy models' used in fitting the observations, are produced by joining power-law segments valid in limiting cases, as described in previous sections. The predictions of such a model could be different from those of a full-featured numerical radiation-hyrodynamic simulation. Some attempts have been made for the latter, though many ingredients have still not been incorporated.

1.9.1 The problem of particle acceleration

DSA in the contest of ultra-relativistic outflows is poorly understood, due mainly to the complexity of the process, and computational difficulties. This forces one to make several assumptions about the microphysics of the shock. From the current understanding of DSA one can not 'derive' ϵ_e, ϵ_B or p from first principles. They, as mentioned in the previous section are inferred from afterglow modelling, and hence depend heavily on the model. In the simple fireball model, ϵ_e, ϵ_B and p are assumed to remain constant throughout the evolution of the shock. This need not be true, but one is left with only conjectures for the time evolution of the shock microphysics.

Due to various levels of assumptions in the standard fireball model, the inferred parameters from a given set of observations could change drastically depending on the afterglow model used. To resolve the problem, more theoretical understanding of particle acceleration mechanism is needed and more detailed modelling of AGs is required. In fact, afterglows are a promising testing ground and input provider for particle acceleration theories.

1.9.2 Non-standard $\alpha - \delta$ Relations

The simple fireball model, could however explain the general features of the observed AGs in the early years. The data set those days were sparse in both temporal and spectral domains. With the availability of more data, model predictions started deviating from the observations. The $\alpha - \delta$ relations described above are derived after making several assumptions and approximations, such as those mentioned in the previous sections. Several afterglows show deviations from the expected $\alpha - \delta$ relations (for eg., GRB050525a [21], GRB050508 [115]) and at times the observed α s and δ s seem to follow none of the regimes the standard model could anticipate. One needs to go beyond the assumptions and simplifications made in the standard model to explain the observed behaviour in these cases.

1.9.3 Hard Electron Energy Spectrum

The assumption of a 'universal powerlaw' (see section 1.8.3) for the accelerated electron distribution does not seem to hold always [122, 145], a fraction of cases appear to exhibit a harder spectrum. In fact, Gamma Ray Bursts or their Afterglows are not the first sources to show evidence of harder electron energy spectra. It is often seen in plerionic supernova remnants like the Crab Nebula.

Hard electron energy spectra require a slightly different approach in deriving the basic equations. The upper cut-off of the distribution can not be neglected, and the expressions for deriving physical parameters are different. We will treat this problem in detail in the chapters to follow.

1.10 The Chapters

In Chapter 2, we present the theoretical modifications to the standard model needed to accommodate electron energy spectra with indices less than 2. The expressions for ν_m and ν_a differ from the standard scenario, as well as a new break ν_i, called the "injection break", is introduced in the spectrum. Both the synchrotron and the inverse compton fluxes are calculated semi-analytically.

For ultra-relativistic and non-relativistic dynamical regimes, analytical solutions are presented. In chapter 3, this model is applied to three AGs (GRB010222, GRB020813 and GRB041006), which have well sampled multi-band lightcurves. We estimate the physical parameters for these afterglows. Chapter 4 and 5 are devoted to GRB030329, one of the best monitored afterglows till date. The 4th Chapter describes the radio observations of the afterglow done with the Giant Meterwave Radio Telescope (GMRT) at low frequencies. This is the longest observed afterglow, as well as the only one which has been observed in frequencies lower than 1 GHz. Thanks to the long coverage, we are able to pin-point the location of ν_a and the transition to the non-relativistic Sedov-Taylor regime. Chapter 5 describes multiband modelling of this afterglow. The multiband evolution of this afterglow had been really complex and a novel suggestion of two concentric jets together giving rise to the observed flux has been made. In this chapter we test the predictions of this conjecture and also suggest a different scenario to explain the observations. Chapter 6, presents the conclusions of the thesis and suggests future directions.